# Full potential *ab initio* calculations of spiral spin density waves in fcc Fe

D. M. Bylander and Leonard Kleinman
*Department of Physics, University of Texas, Austin, Texas 78712-1081*
(Received 28 April 1998; revised manuscript received 3 June 1998)

All *ab initio* calculations of spiral spin density waves heretofore have used the atomic sphere approximation (ASA) in which not only is the potential assumed spherical but also the direction of magnetization is taken constant within each Wigner-Seitz sphere. We have performed full potential local density approximation calculations for $\gamma$-Fe spiral spin density waves with wave vector $\mathbf{q}=(2\pi/a)(0,0,\alpha)$ and $\mathbf{q}=(2\pi/a)(\gamma,0,1)$, finding the ground state at $\alpha\approx 0.55$. The results differ quantitatively but not qualitatively from those of ASA calculations. However, interesting results are obtained for the azimuthal angle of the magnetization $\varphi(\mathbf{r})=\mathbf{q}\cdot\mathbf{r}+\hat{\varphi}(\mathbf{r})$, where $e^{i\hat{\varphi}(\mathbf{r})}$ is a function with the lattice periodicity which is calculated self-consistently. [S0163-1829(98)04738-9]

## I. INTRODUCTION

Very small clusters of fcc Fe ($\gamma$-Fe) can be stabilized as precipitates in a Cu matrix. Larger clusters of fcc $Fe_{97}Co_3$ were also stabilized and in both cases neutron scattering revealed[1] that the low-temperature ground state is a spiral spin density wave with wave vector $\mathbf{q}=(2\pi/a)(0.1,0,1)$. Two different groups[2,3] calculated the total energy for a large number of $\mathbf{q}$'s using the local spin density approximation (LSDA) for exchange and correlation and found over a large range of lattice constants that the ground state is a spiral spin density wave with $\mathbf{q}=(2\pi/a)(0,0,0.6)$. When the generalized gradient approximation[4] (GGA) for exchange and correlation was used,[3] $\mathbf{q}=(2\pi/a)(0,0,0.6)$ remained a local minimum but $\mathbf{q}=(2\pi/a)(0.5,0,1)$ became the ground state. In no case was agreement with experiment obtained. All such calculations have been performed using the atomic sphere approximation (ASA) in which a spherical average of the crystal potential is used within the entire Wigner-Seitz (WS) sphere; moreover, the direction of the spin polarization vector is held fixed within the WS sphere. Therefore it seemed worthwhile to attempt a full potential calculation, not only to determine whether the disagreement between theory and experiment is a consequence of the ASA or an inherent failure of the exchange-correlation approximations but also to determine whether the direction of magnetization changes at a fairly constant rate between atoms or rather abruptly in the region midway between a pair of atoms.

Because the full potential calculations are computationally time consuming, we restrict our calculations in this paper to $\mathbf{q}$'s of the form $(2\pi/a)(0,0,\alpha)$ and $(2\pi/a)(\gamma,0,1)$. In the following section we describe our computational method and the last section contains the results of our calculations along with a discussion thereof.

## II. COMPUTATIONAL METHOD

We start with a $20\times20\times20$ mesh in real space, sampling the fcc unit cell at 8000 points. We will obtain spinor eigenfunctions

$$\begin{pmatrix} \psi_{\uparrow n\mathbf{k}}(\mathbf{r}j) \\ \psi_{\downarrow n\mathbf{k}}(\mathbf{r}_j) \end{pmatrix}$$

at 4000 $\mathbf{k}$ points in the Brillouin zone (BZ) on a $20\times20\times20$ simple cubic mesh,[5] where $n$ is a band index. A lattice translation $\mathbf{R}_j$ followed by an operation which unwinds the spiral spin density wave leaves the crystal invariant. These compound operations form an Abelian group, isomorphic with the group of ordinary translations. Therefore Bloch's theorem holds for these operators, allowing us to sample the ordinary BZ in spite of the fact that the spiral spin density wave is not commensurate with the crystal periodicity.[6,7]

Then averaging over the BZ and summing over bands we evaluate the spin density matrix

$$\rho_{\alpha\beta}(\mathbf{r}_j)=\frac{1}{4000}\sum_{k=1}^{4000}\sum_{n}^{\text{occ}}\psi_{\alpha n\mathbf{k}}(\mathbf{r}_j)\psi^*_{\beta n\mathbf{k}}(\mathbf{r}_j) \tag{1}$$

at all 8000 $\mathbf{r}_j$ in the unit cell. As in Refs. 2, 3, and 8, we diagonalize the spin density matrices obtaining the spin $\frac{1}{2}$ rotation matrix

$$\mathbf{u}(\mathbf{r}_j)=\begin{pmatrix} \exp[i\varphi(\mathbf{r}_j)/2]\cos[\theta(\mathbf{r}_j)/2] & \exp[-i\varphi(\mathbf{r}_j)/2]\sin[\theta(\mathbf{r}_j)/2] \\ -\exp[i\varphi(\mathbf{r}_j)/2]\sin[\theta(\mathbf{r}_j)/2] & \exp[-i\varphi(\mathbf{r}_j)/2]\cos[\theta(\mathbf{r}_j)/2] \end{pmatrix}, \tag{2}$$

 © 1998 The American Physical Society

where the polar angles are given by

$$\cos\ \varphi(\mathbf{r}_j)=\mathrm{Re}\ \rho_{\uparrow\downarrow}(\mathbf{r}_j)/|\rho_{\uparrow\downarrow}(\mathbf{r}_j)|, \tag{3a}$$

$$\sin\ \varphi(\mathbf{r}_j)=-\mathrm{Im}\ \rho_{\uparrow\downarrow}(\mathbf{r}_j)/|\rho_{\uparrow\downarrow}(\mathbf{r}_j)|, \tag{3b}$$

$$\tan\ \theta(\mathbf{r}_j)=2|\rho_{\uparrow\downarrow}(\mathbf{r}_j)|/[\rho_{\uparrow\uparrow}(\mathbf{r}_j)-\rho_{\downarrow\downarrow}(\mathbf{r}_j)]. \tag{3c}$$

In the present case where the magnetization spirals around in the *xy* plane, $\theta(\mathbf{r})=\pi/2$ so that the sine and cosine in Eq. (2) can be replaced by $1/\sqrt{2}$ but $\varphi(\mathbf{r}_j)$ is not merely $\mathbf{q}\cdot\mathbf{R}_j$ as in Refs. 2, 3, 6, and 8 but rather

$$\varphi(\mathbf{r}_j)=\mathbf{q}\cdot\mathbf{r}_j+\hat{\varphi}(\mathbf{r}_j), \tag{4}$$

where $\hat{\varphi}(\mathbf{r}_j)$, which must be evaluated self-consistently, is a function such that $e^{i\hat{\varphi}(\mathbf{r}_j)}$ has the crystal periodicity.

Note that with $\mathbf{z}$ as the quantization direction and the magnetization lying in the *xy* plane, if a given state is occupied, so is its time reversed partner. Then it is trivial to show that $\rho_{\uparrow\uparrow}(\mathbf{r}_j)=\rho_{\downarrow\downarrow}(\mathbf{r}_j)$, consistent with $\theta(\mathbf{r}_j)=\pi/2$ in Eq. (3c).

The diagonalized $\rho_{\alpha\beta}(\mathbf{r}_j)$ takes the form

$$\rho_D(\mathbf{r}_j)=\begin{pmatrix}\rho_{\uparrow\uparrow}(\mathbf{r}_j)+|\rho_{\uparrow\downarrow}(\mathbf{r}_j)| & 0\\ 0 & \rho_{\uparrow\uparrow}(\mathbf{r}_j)-|\rho_{\uparrow\downarrow}(\mathbf{r}_j)|\end{pmatrix}, \tag{5}$$

from which, using the Ceperley-Adler[9] form of LSDA exchange-correlation potential for the full valence plus core charge density, we obtain

$$v_D(\mathbf{r}_j)=\begin{pmatrix}\overline{v}(\mathbf{r}_j)+\Delta v(\mathbf{r}_j) & 0\\ 0 & \overline{v}(\mathbf{r}_j)-\Delta v(\mathbf{r}_j)\end{pmatrix}. \tag{6}$$

We then rotate $v_D(\mathbf{r}_j)$ back to the crystal coordinate system using $\mathbf{u}^{\dagger}(\mathbf{r}_j)$, to obtain[10]

$$v(\mathbf{r}_j)=\begin{pmatrix}\overline{v}(\mathbf{r}_j) & \Delta v(\mathbf{r}_j)e^{-i\varphi(\mathbf{r}_j)}\\ \Delta v(\mathbf{r}_j)e^{i\varphi(\mathbf{r}_j)} & \overline{v}(\mathbf{r}_j)\end{pmatrix}. \tag{7}$$

Then averaging this output potential with the input potential from which our original set of spinor wave functions was obtained, we create a new input Hamiltonian and iterate to self-consistency, just as in ordinary energy band calculations. The calculations are considerably more time consuming than ordinary band calculations for several reasons among which are that both components of the spinor must be expanded in a basis set which doubles the size of the secular equation; to obtain accurate values for the magnetization the calculation must be converged to 0.05 meV in the total energy; the allowed symmetry operations must leave $\mathbf{q}$ unchanged, which increases the number of $\mathbf{k}$ points for which the calculation must be performed.[11]

We used Vanderbilt's[12] ultrasoft pseudopotential, expanding in all plane waves with $(\mathbf{k}+\mathbf{G})^2<40$ Ry. The plane wave charge density contains fourier components up to $2\mathbf{G}_{\max}$ which fits with some room to spare in the $20\times20\times20$ reciprocal space mesh conjugate to our real space mesh. We used one *s*, one *p*, and two *d* projectors. Because the plane wave charge density is not norm conserving, the valence spin density matrix must be reconstructed on the atom in the *m*th unit cell as follows:[12]

$$\hat{\rho}^m_{\alpha\beta}(\mathbf{r})=\rho_{\alpha\beta}(\mathbf{r})+\sum_{s,t}\rho^{\alpha\beta}_{st}(\mathbf{R}_m)Q^{\alpha\beta}_{st}(\mathbf{r}-\mathbf{R}_m), \tag{8}$$

where $\rho_{\alpha\beta}(\mathbf{r})$ is given in Eq. (1),

$$\rho^{\alpha\beta}_{st}(\mathbf{R}_m)=\frac{1}{4000}\sum_{\mathbf{k}=1}^{4000}\sum_{n}^{\mathrm{occ}}\langle\beta_s(\mathbf{r}-\mathbf{R}_m)|\psi_{\alpha n\mathbf{k}}(\mathbf{r})\rangle \times\langle\psi_{\beta n\mathbf{k}}(\mathbf{r})|\beta_t(\mathbf{r}-\mathbf{R}_m)\rangle, \tag{9}$$

$$Q_{st}(\mathbf{r})=\psi^*_s(\mathbf{r})\psi_t(\mathbf{r})-\psi^*_s(\mathbf{r})\varphi_t(\mathbf{r}), \tag{10}$$

$\psi_s(\mathbf{r})$ is an atomic eigenfunction, $\varphi_s(\mathbf{r})$ is the corresponding atomic pseudofunction, $\psi_{\alpha n\mathbf{k}}(\mathbf{r})$ is a spin component of a crystal pseudofunction, and the $|\beta_s\rangle$'s are projectors for the nonlocal part of the pseudopotential. We construct our pseudopotential from a spin unpolarized atom so $Q_{st}(\mathbf{r})$ is the same for both spin components as are the $|\beta_s\rangle$'s. Note that $\rho^{\uparrow\downarrow}_{st}$ contains a phase factor $e^{-i\mathbf{q}\cdot\mathbf{R}_m}$ due to the fact that the individual terms in Eq. (9) can be written $\langle\beta_s(\mathbf{r})|\psi_{\uparrow n\mathbf{k}}(\mathbf{r}+\mathbf{R}_m)\rangle\langle\psi_{\downarrow n\mathbf{k}}(\mathbf{r}+\mathbf{R}_m)|\beta_t(\mathbf{r})\rangle$ and that, because of the form of the potential [Eq. (7)], $\psi_{\uparrow}(\psi_{\downarrow})$ is a Bloch function with a phase factor $e^{i(\mathbf{k}-\mathbf{q}/2)\cdot\mathbf{r}}(e^{i(\mathbf{k}+\mathbf{q}/2)\cdot\mathbf{r}})$. Similarly, $\rho^{\downarrow\uparrow}_{ij}$ contains a factor $e^{i\mathbf{q}\cdot\mathbf{R}_m}$. The integrals in Eq. (9) were all calculated in reciprocal space whereas (unlike Ref. 13) the monopole components of the Coulomb potential arising from the $Q_{st}(\mathbf{r})$ contributions to Eq. (8), as well as other $Q_{st}$ integrals, were calculated on the atomic mesh. The higher Coulomb multipole components were smoothened as in Ref. 13 and evaluated on a $36\times36\times36$ real space mesh. The exchange-correlation potential (and contribution to the total energy) were obtained by evaluating the total (including core) charge density on the $36\times36\times36$ mesh, evaluating the potential (or energy density) on the mesh, fitting in the atomic core region with a spherical function which was Fourier transformed on the atomic mesh while the remainder was fast fourier transformed. All calculations were performed at the lattice constant of the Cu matrix,[14] 6.822 Bohrs. The secular equations were solved using our conjugate gradient method.[15]

## III. RESULTS AND CONCLUSIONS

In Fig. 1 the energy in mRy below the paramagnetic state is shown along $\mathbf{q}=(2\pi/a)(0,0,\alpha)$ and $\mathbf{q}=(2\pi/a)(\gamma,0,1)$. Note $\mathbf{q}=0$ is the ferromagnetic state of which there are two. Our results are quite similar to the ASA calculations[2,3] whose ground state had $\alpha\approx0.6$ compared to our $\alpha\approx0.55$. Although the LSDA is satisfactory for describing ferromagnetic and antiferromagnetic systems we must conclude that it is incapable of yielding the correct spiral spin density wave ground state. The GGA which is better in many respects than the LSDA for ferromagnets and antiferromagnets is not directly applicable to spiral spin density waves (it was easily applied in the ASA because the direction of magnetization was held fixed within the WS sphere); however, it could be applied to the diagonalized spin components of Eq. (5), ignoring the fact that the quantization direction is a function of $\mathbf{r}_j$. Difficulties associated with the fact that $\rho_{\uparrow\downarrow}(\mathbf{r}_j)$ reverses sign in the interstitial regions are easily overcome. We suspect that if the GGA were applied to Eq. (5), the results

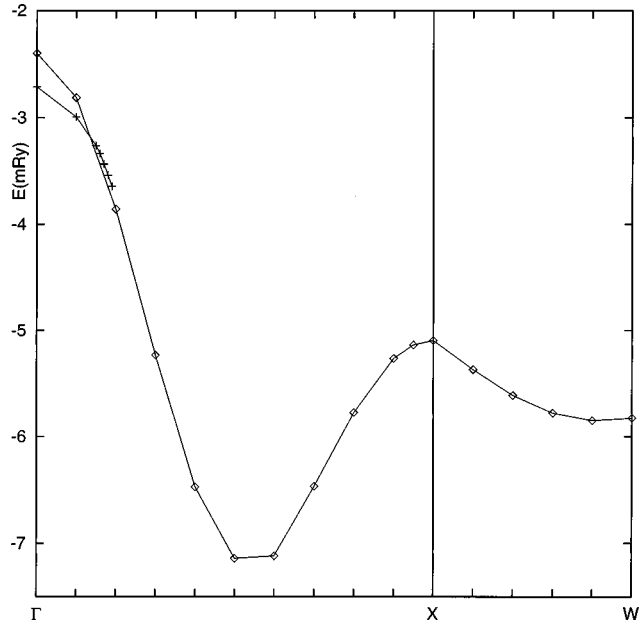


FIG. 1. Energy of the spiral spin density wave for wave vectors along the $\Gamma X$ and $XW$ lines relative to that of nonmagnetic fcc Fe at the same lattice constant. The line denoted by plus symbols is the high spin state.

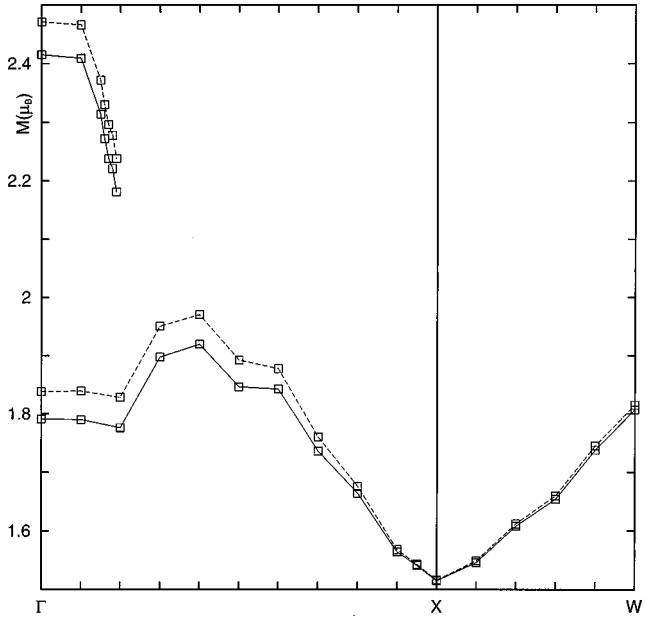


FIG. 2. Integral of the magnitude of the magnetic moment over the Wigner-Seitz cell (dashed line) and of the vector magnetic moment (solid line) for spiral spin density waves for $\mathbf{q}$ along the $\Gamma X$ and $XW$ lines.

would differ from the ASA results by more than they do with the LSDA because in the ASA there are no angular gradients of the charge density. There is, however, no reason to expect the GGA to yield agreement with experiment. The success of the LSDA and GGA for ferromagnets and their failure for spiral spin density waves could be related to the fact that they become exact for ferromagnetic jellium but not for jellium with a spiral spin density wave. Inclusion of the spin-orbit interaction we believe will have only a small effect on these results but even if it is larger than we expect, there is no *a priori* reason why it should minimize the energy at the experimental value of $\mathbf{q}$. On the other hand, there should be a term in the exchange-correlation energy density functional proportional to $|\nabla\varphi|^2$. We have constructed such a term which we will presently show vanishes for $\mathbf{q}=(2\pi/a)\times(0,0,1)$. This term would then favor the energy minimum occurring at or near that $\mathbf{q}$.

Figure 2 contains plots of the magnetization per unit cell evaluated in two ways. The solid line represents the vector magnetization integrated over the Wigner-Seitz cell whereas the dashed line is the integrated magnitude of the magnetization. Note that these differ even for the ferromagnet ($\mathbf{q}=0$) because the minority spin *s* electrons dominate in the interstitial regions and very close to the atomic nuclei.[16] For reasons to become clear presently, we note that this difference vanishes at the *X* point [$\mathbf{q}=(2\pi/a)(0,0,1)$]. Our magnetization curves differ markedly from the ASA curves[2,3] for $q<0.3(2\pi/a)$ and are similar to them for larger $q$. This is a consequence of the ASA high field ferromagnetic state being the same as ours but the ASA low field state having about $0.8\mu_B$ less magnetization than ours. Other ASA calculations[17] find that the low field state only exists over an extremely narrow range of lattice constants (between about 6.84 to 6.87 Bohr). Being so sensitive to the lattice constant, it is likely that its magnitude is sensitive to whatever approximations are made in its calculation. We followed the high field magnetization curve for $\mathbf{q}=(2\pi/a)(0,0,\alpha)$ from $\alpha=0.15$ in steps of 0.01 to $\alpha=0.19$ after which it disappeared, while dropping toward but still well above the low field curve. The ASA calculations found that the low field

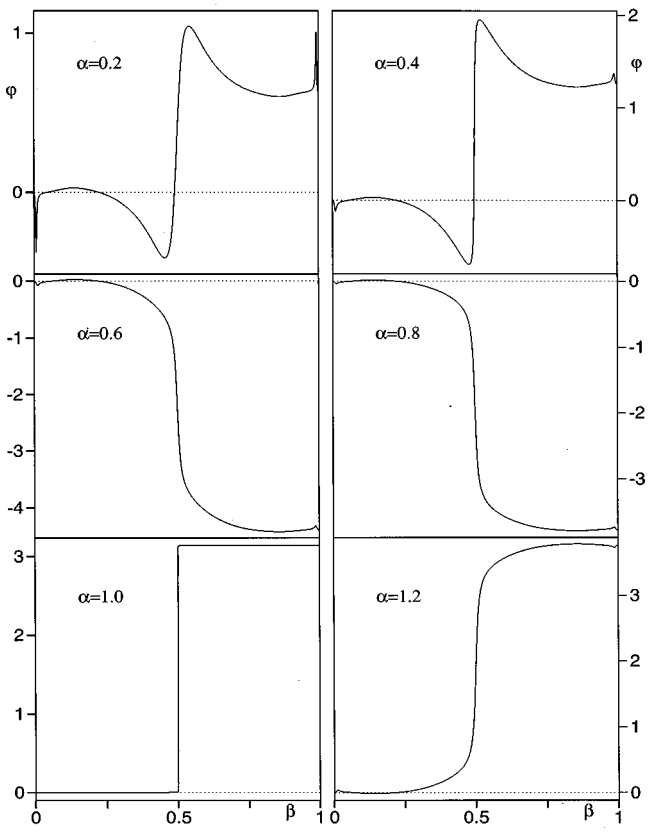


FIG. 3. Phase of the spiral spin density wave $\varphi(\mathbf{r})$ for $\mathbf{q}=(2\pi/a)(0,0,\alpha)$ and $\mathbf{r}=\beta(0,\pm a/2,a/2)$ or $\beta(\pm a/2,0,a/2)$.

curve disappeared at about the same point while rising toward but still well below the high field curve.

Figure 3 contains plots[18] of the phase $\varphi(\mathbf{r})$ for $\mathbf{q}=(2\pi/a)(0,0,\alpha)$ for various values of $\alpha$ and $\mathbf{r}=\beta(0,\pm a/2,a/2)$ or $\mathbf{r}=\beta(\pm a/2,0,a/2)$. In each case the phase shift between nearest neighbors at $\beta=0$ and $\beta=1$ is either $\alpha\pi$ or $\alpha\pi-2\pi$. Depending on the sign of $\mathrm{Re}\,\rho_{\uparrow\downarrow}(\mathbf{r})$, the phase takes the values 0 or $\pi$ whenever $\mathrm{Im}\,\rho_{\uparrow\downarrow}(\mathbf{r})=0$. Note the very sharp peak in $\varphi(\mathbf{r})$ near $\beta=0$ and $\beta=1$ for $\alpha=0.2$. This is a remnant of the fact that in the ferromagnet ($q=0$) the magnetization reverses sign before the first node of the $4s$ functions and is a consequence of $\mathrm{Re}\,\rho_{\uparrow\downarrow}(\mathbf{r})$ becoming extremely small (but not changing sign) at the peak maximum. This peak exists for all $\alpha$ except $\alpha=1$, although it is much smaller for larger $\alpha$. We calculated $\varphi(\mathbf{r})$ for each of the $q$'s indicated in Figs. 1 and 2 and found that for $0.5\leqslant\alpha\leqslant0.95$ it appears as if $\mathbf{q}$ were $(2\pi/a)(0,0,\alpha-2)$. The $-2$, of course, arises from a $(2\pi/a)(0,0,-2)$ reciprocal lattice vector in $\hat{\varphi}(\mathbf{r})$, the part of $\varphi(\mathbf{r})$ that is periodic modulo $2\pi$. Because $\mathbf{q}$ is only defined modulo a reciprocal lattice vector, the $\mathbf{q}=(2\pi/a)(0,0,0.8)$ and $\mathbf{q}=(2\pi/a)(0,0,-1.2)$ states must be degenerate and have identical $\varphi(\mathbf{r})$. This is verified by comparing the $\alpha=0.8$ and $\alpha=1.2$ phase shifts which differ only by a minus sign in Fig. 3. The only unexpected part of this result is that they have a phase shift of $1.2\pi$ rather than $0.8\pi$ between nearest neighbors. Comparing the $\alpha=0.2$ and 0.4 phases one sees that the dip in $\varphi(\mathbf{r})$ before its rapid rise becomes more pronounced with increasing $\alpha$. Thus for larger $\alpha$ the larger but smoother phase shift of $(\alpha-2)\pi$ between neighbors is favored. It seems reasonable that to minimize the energy the phase should be constant where the spin density (which is equal to $2|\rho_{\uparrow\downarrow}(\mathbf{r})|$) is large. This is not possible in general without the $\psi_\uparrow$ and $\psi_\downarrow^*$ from which $\rho_{\uparrow\downarrow}$ is generated having very large kinetic energies. Thus the phases in Fig. 3 are fairly constant where the spin density is largest but are unable to maintain their constant value to the point where the spin density becomes negligible.

One may ask if the change in total phase shift between atoms from $\alpha\pi$ to $(\alpha-2)\pi$ occurs exactly at $\alpha=0.5$ or someplace between $\alpha=0.5$ and $\alpha=0.4$, the closest smaller value of $\alpha$ for which we have performed the calculation. We can see no reason why it should occur exactly at $\alpha=0.5$, however, the phase shift between atoms returns to $\alpha\pi$ at $\alpha=1.0$ exactly. This follows from the fact that $\varphi(\mathbf{r})$ at $\alpha=1-\delta$ equals $-\varphi(\mathbf{r})$ at $\alpha=1+\delta$ and the fact that a $\varphi$ which is constant except for a discontinuous jump of $\pi$ is identical to one where the jump is $-\pi$. When $\mathbf{q}=(2\pi/a)(0,0,1)$ or, for that matter, whenever $\mathbf{q}=\frac{1}{2}\mathbf{G}$ where $\mathbf{G}$ is a reciprocal lattice vector, the phase may be a step function with the step occurring at $\mathbf{R}_m/2$. All that is required is that $\rho_{\uparrow\downarrow}(\mathbf{r})$ have the form $f(\mathbf{r})(1+e^{i\mathbf{G}\cdot\mathbf{r}})e^{-i\mathbf{q}\cdot\mathbf{r}}=2f(\mathbf{r})\cos\frac{1}{2}\mathbf{G}\cdot\mathbf{r}$, where $f(\mathbf{r})$ is a real positive function. Then $\mathrm{Im}\,\rho_{\uparrow\downarrow}(\mathbf{r})=0$ so $\varphi(\mathbf{r})$ must be 0 or $\pi$ and $\mathrm{Re}\,\rho_{\uparrow\downarrow}(\mathbf{r})$ changes sign at $\mathbf{r}=\mathbf{R}_m/2$, causing $\varphi(\mathbf{r})$ to jump discontinuously from 0 to $\pi$ at that point. Because the magnetization does not spiral, but merely reverses sign in this case, the $\mathbf{q}=\mathbf{G}/2$ spiral spin density wave is an antiferromagnetic state. This explains why the two magnetization curves in Fig. 2 become equal at the $X$ point. It also explains why the previously discussed $|\nabla\varphi|^2$ density functional term vanishes at $X$. This term is proportional to $|\rho_{\uparrow\downarrow}\nabla\rho_{\downarrow\uparrow}-\rho_{\downarrow\uparrow}\nabla\rho_{\uparrow\downarrow}|^2$ which at $X$ vanishes everywhere and, in particular, in the plane where $\nabla\varphi$ is infinite. For $\mathbf{r}=\beta(\pm a/2,\pm a/2,0)$, $\mathbf{q}\cdot\mathbf{r}=0$ but also $\hat{\varphi}(\mathbf{r})$ is constant (for any $\alpha$) so the magnetization direction does not even wobble between neighbors in an $xy$ plane.

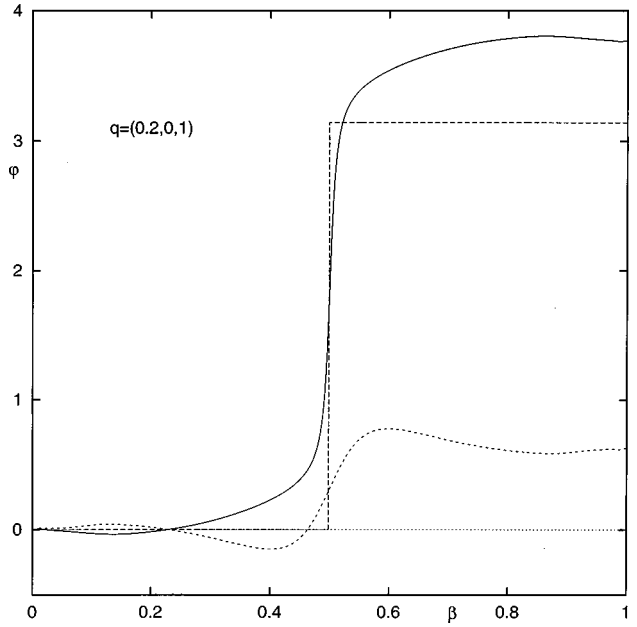


FIG. 4. Phase of the spiral spin density wave $\varphi(\mathbf{r})$ for $\mathbf{q}=(2\pi/a)$ (0.2,0,1) and for $\mathbf{r}=\beta(0,\pm a/2,\pm a/2)$ (long dashes), $\mathbf{r}=\beta(a/2,\pm a/2,0)$ (short dashes), and $\mathbf{r}=\beta(a/2,0,\pm a/2)$ (solid line).

We have also performed a standard calculation of an antiferromagnetic state starting from a superposition of atomic spin densities alternating in direction on alternate (0,0,1) atomic planes. This converges to a state which is unrelated to the $\alpha=1$ antiferromagnetic state. It lies above it in energy, 3.81 mRy below the nonmagnetic state. Its spin density is drastically different. If we call the atom at (0,0,0) a spin up atom, then $(0,0,a/2)$ is an octahedral point, equidistant from four spin down atoms in the $(0,0,a/2)$ plane at $(\pm a/2,0,a/2)$ and $(0,\pm a/2,a/2)$ and two spin up atoms at (0,0,0) and $(0,0,a)$. In the $\alpha=1$ antiferromagnet the spin density is down at $(0,0,a/2)$ but in the standard antiferromagnet it is up, i.e., it is opposite to the spin of a majority of its nearest neighbors. This is less surprising when one notes that at the octahedral point in the ferromagnet the minority spins dominate.

We have also examined the $\varphi(\mathbf{r})$ for $\mathbf{q}=(2\pi/a)(\gamma,0,1)$ and plot it in Fig. 4 for $\gamma=0.2$ along inequivalent nearest neighbor directions. For $\mathbf{r}=\beta(0,\pm a/2,\pm a/2)$, $\varphi(\mathbf{r})$ is a step function of height $\pi$, i.e., the $x=0$ plane is antiferromagnetic. For $\mathbf{r}=\beta(a/2,\pm a/2,0)$ the total phase shift between nearest neighbors is $\gamma\pi$. For $\mathbf{r}=\beta(a/2,0,a/2)$ the phase shift is $(1+\gamma)\pi$ between neighbors and for $\mathbf{r}=\beta(a/2,0,-a/2)$ it is $(\gamma-1)\pi+2\pi=(1+\gamma)\pi$. Thus the $x=a/2$ plane is antiferromagnetic but with the spins rotated by $\gamma\pi$ and $(1+\gamma)\pi$ relative to the atom at (0,0,0). At $W$, however, the phase shift between nearest neighbors for both $\mathbf{r}=\beta(a/2,0,a/2)$ and $\mathbf{r}=\beta(a/2,0,-a/2)$ is $-0.5\pi$ rather than the $1.5\pi$ one would have predicted from the $\gamma<0.5$ results.

Thus for $\mathbf{q}=(2\pi/\alpha)(\gamma,0,1)$ the crystal is best described as being antiferromagnetic in *yz* planes of atoms with the quantization axis rotating through $\gamma\pi$ between atomic planes. When $\gamma=0$ this is better described as ferromagnetic *xy* planes of atoms with the magnetization reversing sign midway between planes.

In conclusion, we have calculated the properties of fcc iron in its spiral spin density wave ground state without any potential or magnetization direction approximations. Other than differences in the low spin ferromagnetic state which extend out to $q=0.3(2\pi/a)$ our magnetization vs wave vector curves are qualitatively the same as those obtained from ASA calculations whereas our energy vs wave vector curves are qualitatively the same for all **q**. Since these fail to yield the experimental ground state **q**, we have concluded that current exchange-correlation approximations are inadequate. We note that the LSDA only distinguishes between up and down spins at a point in space and is completely oblivious to the fact that the local quantization direction is a function of position; furthermore there does not appear to be a uniquely correct way to apply the GGA to this case. Our study of the phase shifts revealed three facts that had not previously been appreciated. (1) When the phase shift between neighboring atoms is $\pi$, the entire phase shift occurs discontinuously midway between atoms where the spin density vanishes, i.e., the $\mathbf{q}=\frac{1}{2}\mathbf{G}$ spiral spin density wave *is* an antiferromagnetic state although not the usual one. (2) The phase is a highly nonmonotonic function for $\alpha<0.5$. (3) Although the smallest possible spin rotation between neighboring atoms is $\alpha\pi$ with $\alpha<1$, the system chooses the larger rotation of $(\alpha-2)\pi$ as its ground state for $0.5\leqslant\alpha<1$. Since the spin density polarization is a continuous function (except for $\alpha=1$), these two rotations are not equivalent.

## ACKNOWLEDGMENTS

These calculations were performed at the Texas Advanced Computing Center of the University of Texas at Austin and supported by the University and NPACI. The research was supported by the Welch Foundation (Houston, TX) and the NSF under Grant No. DMR-9614040.

[1] Y. Tsunoda, Y. Nishioka, and R. M. Nicklow, J. Magn. Magn. Mater. **128**, 133 (1993).

[2] M. Uhl, L. M. Sandratskii, and J. Kübler, J. Magn. Magn. Mater. **103**, 314 (1992).

[3] M. Körling and J. Ergon, Phys. Rev. B **54**, 8293 (1996).

[4] J. P. Perdew, in *Electronic Structure of Solids 1991*, edited by P. Ziesche and H. Eschrig (Akademie Verlag, Berlin, 1991), Vol. 11.

[5] This set of points fills a cube which contains the first two BZ, hence 8000/2 points in the first BZ. That our real space and BZ meshes are both $20\times20\times20$ is pure coincidence. Note that the real space mesh is defined with respect to three principle lattice vectors and is not cubic.

[6] M. Uhl, L. M. Sandratskii, and J. Kübler, Phys. Rev. B **50**, 291 (1994).

[7] Conyers Herring, *Magnetism*, edited by George T. Rado and Harry Suhl (Academic, New York, 1966), Vol. IV.

[8] J. Sticht, K.-H. Höck, and J. Kübler, J. Phys.: Condens. Matter **1**, 8155 (1989).

[9] D. M. Ceperley and B. J. Alder, Phys. Rev. Lett. **45**, 566 (1980).

[10] Note from Eq. (3) that $e^{-i\varphi(\mathbf{r}_j)}=\rho_{\uparrow\downarrow}/|\rho_{\uparrow\downarrow}|$ so that the phase angles need not be explicitly calculated.

[11] For $\mathbf{q}=(0,0,0)$ the 4000 BZ **k** points reduce to 110 in the $\frac{1}{48}$th irreducible wedge. For $\mathbf{q}=(0,0,\alpha)$ this becomes 275 **k** points in the $\frac{1}{16}$th irreducible wedge. To obtain this reduction time reversal as well as spatial symmetry must be used. For $\mathbf{q}=(2\pi/a)(\alpha,0,1)$ the symmetry operations become complicated because of required reciprocal lattice vector translations, e.g., under $q_z\rightarrow-q_z$, $q_y\rightarrow q_y$, $q_x\rightarrow q_x$, **q** goes into itself modulo the $(2\pi/a)(0,0,2)$ reciprocal lattice vector. Because of the form of $v(\mathbf{r}_j)$ in Eq. (7), the upper and lower components of the eigenspinors have wave vectors $(\mathbf{k}\mp\mathbf{q}/2)$. Let us consider $\mathbf{k}=(2\pi/a)(\frac{1}{8},\frac{1}{8},\frac{1}{8})$. Then under reversal of the sign of $(k_z+q_z/2)$, $(\mathbf{k}+\mathbf{q}/2)\rightarrow(2\pi/a)[(\frac{1}{8},\frac{1}{8},-\frac{1}{8})+\frac{1}{2}(\alpha,0,-1)]$ $=(2\pi/a)\,[(\frac{1}{8},\frac{1}{8},-\frac{9}{8})+\frac{1}{2}(\alpha,0,1)]\rightarrow(2\pi/a)(\frac{1}{8},\frac{1}{8},\frac{7}{8})+\mathbf{q}/2$. Similarly $(\mathbf{k}-\mathbf{q}/2)\rightarrow(2\pi/a)(\frac{1}{8},\frac{1}{8},\frac{7}{8})-\mathbf{q}/2$ so that $\mathbf{k}=(2\pi/a)(\frac{1}{8},\frac{1}{8},\frac{7}{8})$ is a degenerate partner of $\mathbf{k}=(2\pi/a)\times(\frac{1}{8},\frac{1}{8},\frac{1}{8})$ and may be obtained from it. There are 500 independent **k**'s when $\mathbf{q}=(2\pi/a)(\alpha,0,1)$ but only 275 when $\alpha=\frac{1}{2}$.

[12] David Vanderbilt, Phys. Rev. B **41**, 7892 (1990).

[13] K. Laasonen, A. Pasquarello, R. Car, C. Lee, and D. Vanderbilt, Phys. Rev. B **47**, 10 142 (1993).

[14] Charles Kittel, *Introduction to Solid State Physics*, 7th ed. (Wiley, New York, 1996).

[15] D. M. Bylander, Leonard Kleinman, and Seongbok Lee, Phys. Rev. B **42**, 1394 (1990), Appendix A.

[16] The majority spin *s* electrons find the region where the 3*d* charge density is large much more attractive than do the minority spin *s* electrons, leaving the minority spin density larger elsewhere.

[17] V. L. Moruzzi, P. M. Marcus, K. Schwarz, and P. Mohn, Phys. Rev. B **34**, 1784 (1986).

[18] Although the calculation is performed on a $20\times20\times20$ mesh, using the plane wave expansion of the ''smooth'' part of $\rho_{\uparrow\downarrow}(\mathbf{r})$ we are able to evaluate it at any **r**. The supplemental charge in Eq. (8) has its spherical component on the atomic mesh which is easily interpolated to the set of points used to draw Fig. 3 while its nonspherical part is on the $36\times36\times36$ mesh. Its fast fourier transform is then used to interpolate to the points used in Fig. 3.